JOURNAL OF Materials CHEMISTRY

Structure–property correlations in the new ferroelectric $Bi_5PbTi_3O_{14}Cl$ and related layered oxyhalide intergrowth phases

Ardak M. Kusainova,[a] Sergei Yu. Stefanovich,[b] John T. S. Irvine[a] and Philip Lightfoot*[a]

[a]*School of Chemistry, University of St Andrews, St Andrews, Fife, UK KY16 9ST. E-mail: pl@st-and.ac.uk*
[b]*Karpov Institute of Physical Chemistry, 10, Vorontsovo Pole, 103064 Moscow, Russia*

Received 23rd August 2002, Accepted 9th September 2002
First published as an Advance Article on the web 30th October 2002

The crystal structure and electrophysical properties of the layered intergrowth phase $Bi_5PbTi_3O_{14}Cl$ have been studied using powder neutron diffraction, ac impedance and second harmonic generation methods. This phase adopts a structure based on a regular intergrowth of Aurivillius-like and Sillén-like blocks in the layer sequence $\cdots[M_2O_2][M_2Ti_3O_{10}][M_2O_2][Cl]\cdots$, and is therefore closely structurally related to the well-known ferroelectric $Bi_4Ti_3O_{12}$. The phase adopts the polar orthorhombic space group *P*2*an* at temperatures below 590 °C, and transforms directly to a centrosymmetric tetragonal phase, space group *P*4/*mmm*, at that temperature. This abrupt structural phase transition is consistent with a sudden loss of SHG signal and a dielectric maximum at the same temperature. The structural features and electrophysical behaviour of this phase in relation to $Bi_4Ti_3O_{12}$ and related layered oxides/oxyhalides are discussed.

Introduction

Ferroelectrics of the Aurivillius family[1] have recently enjoyed a renaissance due to the observation of fatigue-free properties in their thin film forms, making them candidates for ferroelectric information storage applications.[2] The Aurivillius phases consist of a regular layered intergrowth of alternating fluorite-like $[Bi_2O_2]^{2+}$ and perovskite-like $[A_{n-1}B_nO_{3n+1}]^{2-}$ blocks, examples being $SrBi_2Ta_2O_9$ ($n = 2$) and $Bi_4Ti_3O_{12}$ ($n = 3$). These compounds adopt tetragonal, or pseudo-tetragonal, crystal structures with the *a* and *b* parameters being dictated by the 'width' of the fluorite and perovskite units, and the *c* parameter dependent on the number and type of blocks in the repeat unit. The existence and extent of compositional stability of phases of this type depends critically on the size compatibility of the two types of intergrown block, in particular, the 'matching' of the *a* and *b* unit cell parameters of these units. Similar considerations have been used, for example, in explaining phase stabilities in a related series of layered oxychalcogenides MOCuX (M = Bi, Ln; X = S, Se, Te).[3] In the case of the Aurivillius phases, it is the distortions, *i.e.* polyhedral rotations and cation displacements, required to accommodate the size mismatch which produce the crystal-chemical opportunity for the widespread occurrence of ferroelectricity in these materials.

It is now well established that building blocks other than perovskite-like ones may also intergrow with the $[Bi_2O_2]^{2+}$ unit to generate similar regular intergrowth phases. For example, halide layers generate the Sillén family $[M_2O_2]X_m$, where M = Bi^{3+}, Pb^{2+} *etc.*, X is a halide and $m = 1$–3.[4] CsCl-like blocks have also been shown to intergrow to produce a third series.[5,6] Of particular relevance to the present work is the scope for preparing *triple* intergrowths, of alternating fluorite, perovskite and halide layers, of general composition $[M_2O_2][A_{n-1}B_nO_{3n+1}][M_2O_2][X_m]$. The nomenclature A*n*X*m* is used for these phases, where *n* represents the number of perovskite octahedral layers and *m* the number of halide layers, *e.g.* Bi_4NbO_8Cl represents the archetypal A1X1 member. These phases were first proposed, with preliminary crystallographic characterisation, by Ackerman[7] and by Aurivillius.[8] Our own recent work has now extended these earlier studies to more detailed crystallographic characterisation, and, additionally, to the observation that ferroelectricity is also widespread in this family.[9–11]

One of our motivations for studying these more complex layered intergrowths lies in the idea that the electrophysical properties are determined by crystallographic effects dictated by the requirements for these differing building blocks to achieve structural compatibility in the intergrowth. This follows on from the simple, well-established concept of the 'tolerance factor' in perovskite chemistry,[12] which predicts structural distortion due to the differing sizes of the 'AO' and 'BO_2' layers of the ABO_3 perovskite unit. This concept has already been suggested as a factor in determining the ferroelectric Curie temperature, T_C, in the Aurivillius phases themselves.[13] However, in these complex layered intergrowths, it is not only the 'tolerance' of the A and B perovskite sites which must be considered, but the additional 'tolerance' of the $[A_{n-1}B_nO_{3n+1}]$ *versus* $[M_2O_2]$ and/or $[X_m]$ layers. As a preliminary study of the structural and property influences produced by this additional complexity, we have recently reported unusual 'relaxor'-type ferroelectric properties in the A2X1 phase $Bi_3Pb_2Nb_2O_{11}Cl$.[10] Here we extend our studies to the next homologue, the A3X1 phase $Bi_5PbTi_3O_{14}Cl$, ideally representing the regular intergrowth '$[Bi_4Ti_3O_{12}][BiPbO_2Cl]$', and provide a comparison with the behaviour of the Aurivillius phase $Bi_4Ti_3O_{12}$ itself.

Experimental

$Bi_5PbTi_3O_{14}Cl$ was prepared from Bi_2O_3 (99.9%), BiOCl (99%), TiO_2 (99.9%) and PbO (99.9%), and obtained as a polycrystalline yellow powder. A stoichiometric mixture of the appropriate ingredients was well ground in an agate mortar and heated in a sealed silica ampoule, evacuated under 10^{-2} mmHg pressure, with a final annealing temperature of 820 °C for 20 h. The phase purity of the compound was monitored on a Stoe STADI/P powder X-ray diffractometer operating in transmission mode and utilising monochromated Cu-$K_{\alpha 1}$ radiation.

Powder neutron diffraction

Powder neutron diffraction (PND) data were collected on the high flux diffractometer POLARIS (at temperatures of 100–700 °C in 50 °C steps) and the high resolution diffractometer HRPD (at 25 °C) at the ISIS facility (Rutherford Lab, Chilton, UK) which operates in energy-dispersive (time-of-flight) mode. Approximately 5 g of the sample was placed in a cylindrical vanadium can and data were collected for 3 h on HRPD or 1 h per temperature on POLARIS. Rietveld analysis was carried out using the GSAS package.[14]

Second harmonic generation tests, thermal analysis and dielectric measurements

Impedance measurements were performed with a Solartron 1260 frequency response analyser, using Zplot and Zview impedance software (Scribner). A pellet of diameter 13 mm and thickness 2–3 mm was prepared by pressing (3 t) the powdered $Bi_5PbTi_3O_{14}Cl$ with a little poly(vinyl alcohol) (3% aqueous solution). Pellets suitable for electrophysical measurements were prepared by pasting electrodes [Au paste (Engelhard)] on both sides (electrical resistance 2–5 Ω) and annealing at 600 °C for several hours in air. The maximum sample density achieved was approximately 70% of the theoretical value. The dielectric constant and electrical conductivity were measured between 320–600 °C with PC-controlled ac bridges in the frequency range 10^{-1}–10^{7} Hz. Differential themal analysis (DTA) measurements were recorded on a TA Instruments SDT 2960 thermal analyzer, under N_2, with a scan rate of 10 °C min^{-1}.

Second harmonic generation (SHG) tests were carried out in the range 25–700 °C using a Nd:YAG solid-state laser operating at a wavelength of $\lambda_\omega = 1.064$ μm in the Q-switching mode with a repetition rate of 4 Hz. Light emission at $\lambda_{2\omega} = 0.532$ μm from the surface of the ceramic samples was measured in reflection relative to the SHG signal from a finely powdered SiO_2 standard.

Results and discussion

SHG, DTA and dielectric characterisation

SHG data for $Bi_5PbTi_3O_{14}Cl$ are shown in Fig. 1, with a comparative plot of the corresponding data for $Bi_4Ti_3O_{12}$. The large SHG signals observed at room temperature confirm the non-centrosymmetric nature of both materials. An abrupt loss of the SHG signal is seen for both samples, indicative of a phase transition to a centrosymmetric phase at temperatures of ~590 and ~675 °C for $Bi_5PbTi_3O_{14}Cl$ and $Bi_4Ti_3O_{12}$, respectively. The value for $Bi_4Ti_3O_{12}$ is consistent with the known T_C for this material. In the case of $Bi_4Ti_3O_{12}$, a clear endothermic event in the DTA trace is seen coincident with T_C, confirming a first-order transition. For $Bi_5PbTi_3O_{14}Cl$ however, no thermal event could be detected, suggesting a somewhat 'smeared' transition, though the PND data reported below do suggest a discontinuous transition at T_C.

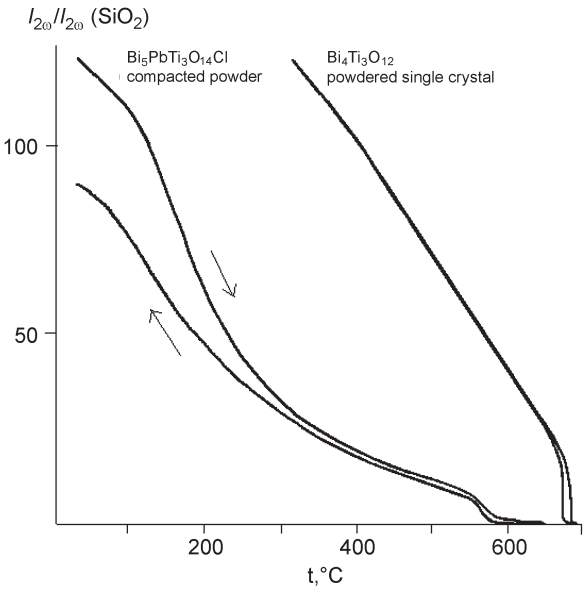

Fig. 1 SHG response for $Bi_5PbTi_3O_{14}Cl$ *vs.* $Bi_4Ti_3O_{12}$.

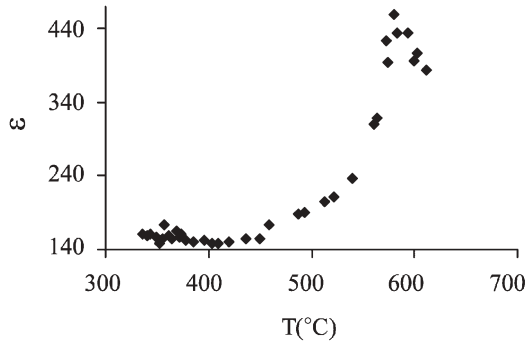

Fig. 2 Temperature dependence of the dielectric constant for $Bi_5PbTi_3O_{14}Cl$.

The dielectric data show a ferroelectric-like permittivity maximum around 590 °C (Fig. 2) with a peak relative permittivity of around 450.

Crystal structure of $Bi_5PbTi_3O_{14}Cl$ at 25 °C

Preliminary examination of the powder X-ray diffraction data suggested that this phase could be indexed based on an orthorhombic unit cell of approximately 5.49 × 5.46 × 22.4 Å. This cell appeared C-centred from X-ray data alone. However, careful analysis of the raw neutron data revealed several reflections which violated C-centring. Systematic absences were compatible with space group *P2an* (no. 30), which is a polar subgroup of *C2mm* (no. 38). Moreover, this space group had also been suggested as an ideal model for a 'mixed odd-layer' Aurivillius phase of the type A1A3,[15] which might be expected to be architecturally similar to the present phase. Refinement of the structure at 25 °C was therefore carried out in this space group using a model derived from that of Aurivillius in *C2mm*.[8] In the final refinement cycles, oxygen atoms of the perovskite block were refined anisotropically and all other atoms isotropically. No attempt was made to determine the location of Pb *vs.* Bi, as these have similar neutron scattering lengths (Pb: 0.94; Bi: 0.85 × 10^{-12} cm). The final refinement converged to $\chi^2 = 4.1$, $R_{wp} = 0.085$ for 81 variables, as compared to 10.1

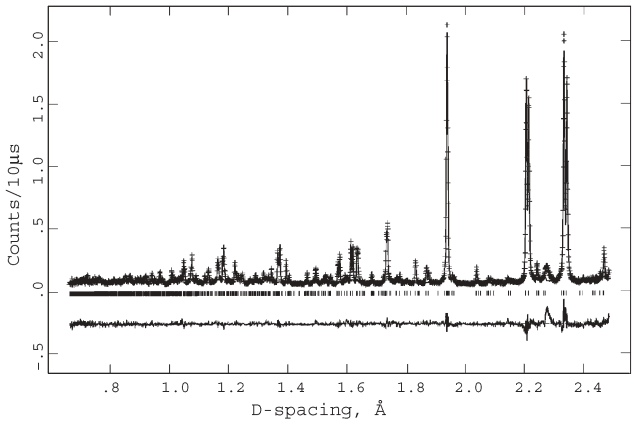

Fig. 3 Final Rietveld plot for $Bi_5PbTi_3O_{14}Cl$ at 25 °C; space group *P2an*.

Table 1 Final atomic parameters and anisotropic thermal parameters for $Bi_5PbTi_3O_{14}Cl$ at 25 °C; space group *P2an*, $a = 5.4940(1)$, $b = 5.4618(1)$, $c = 22.4111(5)$ Å

Atom	*x*	*y*	*z*	U_{iso} (equiv)/Å^2	*U*(11)/Å^2	*U*(22)/Å^2	*U*(33)/Å^2	*U*(12)/Å^2	*U*(13)/Å^2	*U*(23)/Å^2
Bi(1)	0.014(3)	−0.005(1)	0.4145(2)	0.012(1)						
Bi(2)	0.0[a]	0.504(1)	0.0963(2)	0.026(1)						
Bi(3)	0.009(3)	0.491(1)	0.3012(2)	0.027(1)						
Ti(1)	0.042(5)	0.0	0.0	0.009(2)						
Ti(2)	0.045(3)	−0.010(3)	0.1856(3)	0.009(2)						
Cl(1)	0.013(3)	0.5	0.5	0.021(1)						
O(1)	−0.024(5)	−0.050(2)	0.0861(4)	0.060*	0.09(1)	0.07(1)	0.022(4)	−0.01(1)	0.01(1)	−0.010(6)
O(2)	0.024(4)	0.047(2)	0.2639(4)	0.041*	0.069(7)	0.012(6)	0.042(4)	−0.01(1)	−0.046(8)	0.00(4)
O(3)	0.305(3)	0.228(2)	0.0039(9)	0.044*	0.055(8)	−0.007(4)	0.085(7)	0.005(5)	−0.031(1)	0.002(8)
O(4)	0.268(3)	0.237(3)	0.3620(4)	0.010(2)						
O(5)	0.276(3)	0.237(2)	0.1629(5)	0.034*	0.038(7)	0.002(5)	0.064(8)	−0.013(5)	0.037(8)	−0.035(7)
O(6)	0.730(4)	0.769(4)	0.1779(5)	0.077*	0.13(2)	0.07(1)	0.027(6)	−0.06(1)	−0.04(1)	0.03(1)
O(7)	0.794(3)	0.744(2)	0.3621(4)	0.010(2)						

[a]Fixed to define origin of polar axis.

and 0.134, respectively, for the best *C2mm* model (Fig. 3). The structure of this model is shown in Fig. 4, with final refined coordinates and bond lengths reported in Tables 1 and 2, respectively.

The *P2an* structure exhibits the anticipated structural features of a regular intergrowth of $[(Pb/Bi)_2O_2]$, $[(Pb,Bi)_2Ti_3O_{10}]$ and [Cl] blocks. This lower symmetry space group also allows tilting of the TiO_6 octahedra, as well as cooperative atomic displacements along the polar *a* axis. The nature of the tilts is similar to that observed in the corresponding Aurivillius phase $Bi_4Ti_3O_{12}$.[16–18] Neighbouring TiO_6 octahedra along the *a* and *b* crystallographic axes are *oppositely* tilted (*i.e.* out-of-phase tilting), whereas along the *c* axis, the two outer $[Ti(2)O_6]$ octahedra tilt in anti-phase, the inner $[Ti(1)O_6]$ octahedron is constrained by the 2-fold axis to be untilted. This situation is most similar to the $a^-b^-b^-$ system in the Glazer notation for 3-dimensional perovskites.[19] This is contrary to the situation in 'even-layer' Aurivillius phases, such as $SrBi_2Ta_2O_9$[20,21] and $SrBi_4Ti_4O_{15}$,[22] where the ferroelectric phase adopts space group $A2_1am$—the presence of the mirror symmetry relative to the *c* axis dictates in-phase tilting of the two central BO_6 octahedra along that direction, but allows out-of-phase tilting between inner and outer layers. Moreover, subtle

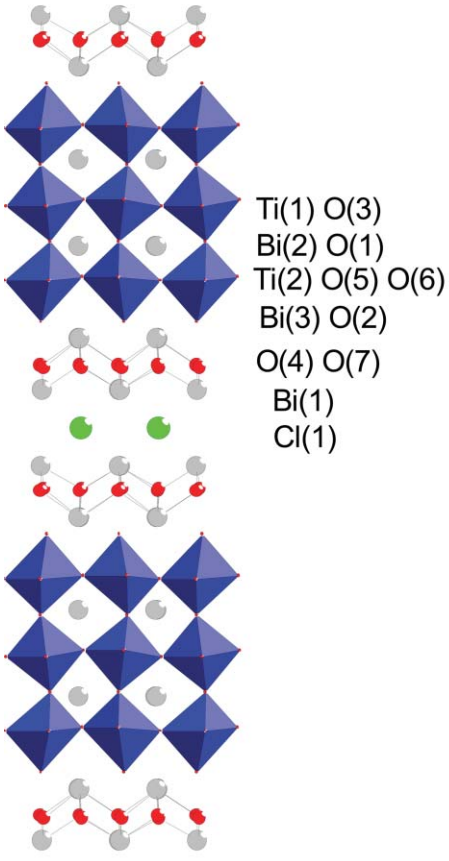

Fig. 4 Crystal structure of $Bi_5PbTi_3O_{14}Cl$ at 25 °C viewed along [110]; space group *P2an*.

Table 2 Comparison of bond lengths (Å) and angles (degrees) in $Bi_5PbTi_3O_{14}Cl$ and $Bi_4Ti_3O_{12}$ at 25 °C

	$Bi_5PbTi_3O_{14}Cl$	$Bi_4Ti_3O_{12}$ (ref. 18)[a]
Ti(1)–O(1) × 2	1.98(1)	1.99(1)
Ti(1)–O(3) × 2	1.91(2)	1.88(1)
Ti(1)–O(3) × 2	1.98(2)	1.99(1)
Ti(2)–O(1)	2.27(1)	2.32(1)
Ti(2)–O(2)	1.79(1)	1.75(1)
Ti(2)–O(5)	1.92(2)	2.00(2)
Ti(2)–O(5)	2.16(2)	2.03(2)
Ti(2)–O(6)	1.75(2)	1.87(2)
Ti(2)–O(6)	2.11(2)	2.06(2)
Bi(1)–O(4)	2.25(1)	—
Bi(1)–O(4)	2.31(1)	—
Bi(1)–O(7)	2.17(1)	—
Bi(1)–O(7)	2.33(1)	—
Bi(1)–Cl(1)	3.31(1)	—
Bi(1)–Cl(1)	3.34(1)	—
Bi(1)–Cl(1)	3.36(1)	—
Bi(1)–Cl(1)	3.36(1)	—
Bi(2)–O(1)	2.45(1)	2.31(1)
Bi(2)–O(1)	2.64(2)	2.42(1)
Bi(2)–O(1)	2.90(2)	3.10(1)
Bi(2)–O(1)	3.04(1)	3.21(1)
Bi(2)–O(3)	2.66(2)	2.56(1)
Bi(2)–O(3)	2.77(2)	2.96(1)
Bi(2)–O(3)	3.06(2)	2.97(1)
Bi(2)–O(3)	3.16(2)	3.32(1)
Bi(2)–O(5)	2.34(1)	2.36(1)
Bi(2)–O(5)	2.58(2)	2.46(1)
Bi(2)–O(6)	2.55(2)	2.33(1)
Bi(2)–O(6)	2.76(2)	3.20(1)
Bi(3)–O(2)	2.57(1)	2.58(1)
Bi(3)–O(2)	2.80(2)	2.61(1)
Bi(3)–O(2)	2.96(2)	3.12(1)
Bi(3)–O(2)	3.15(1)	3.20(1)
Bi(3)–O(4)	2.27(2)	2.19(1)
Bi(3)–O(4)	2.41(1)	2.31(1)
Bi(3)–O(7)	2.27(1)	2.26(1)
Bi(3)–O(7)	2.53(1)	2.46(1)
Ti(1)–O(1)–Ti(2)	156(1)	159(1)
Ti(1)–O(3)–Ti(1)	171(1)	164(1)
Ti(2)–O(6)–Ti(2)	158(1)	152(1)
Ti(2)–O(5)–Ti(2)	151(1)	147(1)

[a]The results reported in ref. 18 override those in ref. 17.

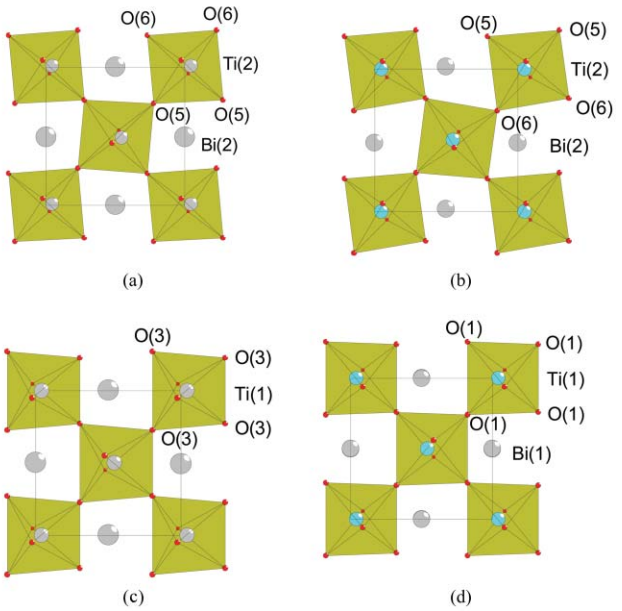

Fig. 5 Projections of the BO_6 octahedral layers down the *c* axis: (a) $Bi_5PbTi_3O_{14}Cl$, Ti(2) layer; (b) $Bi_4Ti_3O_{12}$, Ti(2) layer; (c) $Bi_5PbTi_3O_{14}Cl$, Ti(1) layer; (d) $Bi_4Ti_3O_{12}$, Ti(1) layer.

differences exist between the precise nature of the distortions in $Bi_5PbTi_3O_{14}Cl$ and $Bi_4Ti_3O_{12}$. Calculation of a total spontaneous polarisation, P_s, using a simple point charge model[23] gives a value of only 4.2 μC cm^{-2} for $Bi_5PbTi_3O_{14}Cl$, compared to ~36 μC cm^{-2} for $Bi_4Ti_3O_{12}$.[18,23] The structural difference can be traced to the atomic displacements within the perovskite blocks in the two structures, which are shown in Fig. 5. The figure shows plan views, down the *c* axis, of each of the TiO_6 octahedral layers for both $Bi_5PbTi_3O_{14}Cl$ and $Bi_4Ti_3O_{12}$. It can be seen that, within the outer Ti(2)O_6 layer, the degree of rotation around the *c* axis is greater for $Bi_4Ti_3O_{12}$, whereas the degree of displacement of Ti(2) itself from the centre of the octahedron towards an O(5)–O(6) edge is larger for $Bi_5PbTi_3O_{14}Cl$. However, this does not increase the overall polarisation along *a*, as the net charge separation of this octahedral oxygen environment relative to the Bi(2) origin is correspondingly smaller. A similar situation occurs for the Ti(1)O_6 layer. These differences are also manifest in the atomic coordinates (Table 1). Displacements, Δx, along the polar *a* axis relative to the fixed origin at Bi(2) are positive for all atoms, except O(1) and O(6) (relative to the ideal positions at $x = 0, 0.25, 0.75$). In the case of $Bi_4Ti_3O_{12}$, *all* such Δx deviations are positive, leading to a much larger overall polarisation.

Some insight into the effects of the relative structural compatibility of the Sillén and Aurivillius-like intergrowth units can be gleaned from comparision of the present example with our previous work on the A2X1 phase $Bi_3Pb_2Nb_2O_{11}Cl$.[10] Table 3 shows the *a* and *b* lattice parameters of these two intergrowth phases together with those of the idealised constituent Sillén and Aurivillius phases. It can be seen that the lattice parameters of the 'pure' Sillén X1 block, $PbBiO_2Cl$, are much larger than either of the required A2 or A3 blocks. In the case of the hypothetical A2 → A2X1 transformation, the additional strain exerted on the A2 block in accommodating the X1 block is sufficient to lead to a complete loss of long range octahedral tilting in $Bi_3Pb_2Nb_2O_{11}Cl$, and apparent *P*4/*mmm* symmetry in the ferroelectric structure. We previously retaionalised this by proposing the existence of polar nanodomains too small to see in a neutron or X-ray diffraction experiment.[10] In the case of the A3 → A3X1 transformation however, the *a* and *b* parameters of the constituent A3 and X1 blocks are even less well matched and the net result, as shown here, is a compromise A3X1 phase with some degree of long range octahedral tilting still retained, albeit with a calculated overall spontaneous polarisation which is much reduced from that of the 'pure' A3 phase, $Bi_4Ti_3O_{12}$. Considering these dramatic structural effects, it is perhaps surprising that the resultant values of T_C differ by relatively modest amounts between the A*n* and A*n*X1 phases studied so far. Early studies suggested correlations between both P_s and T_C, and P_s and SHG intensity in various classes of ferroelectric materials.[24] Experimental measurement of P_s in the A*n*X1 materials is required in order to understand this behaviour further.

Table 3 Comparison of *a* and *b* unit cell parameters at 25 °C (Å) and T_C for layered phases containing A2, A3 and X1 blocks

Compound	Type	*a*/Å	*b*/Å	T_C/°C	Ref.
$PbBiO_2Cl$	X1	5.593	5.558	—	26
$PbBi_2Nb_2O_9$	A2	5.504	5.487	560–610	27
$Bi_4Ti_3O_{12}$	A3	5.445	5.410	670	18
$Bi_3Pb_2Nb_2O_{11}Cl$	A2X1	'5.530'[a]	5.530	410	10
$Bi_5PbTi_3O_{14}Cl$	A3X1	5.494	5.462	591	This work

[a]True value: 3.910 ($= a/\sqrt{2}$).

Thermal evolution of the structure of $Bi_5PbTi_3O_{14}Cl$

Both the dielectric and SHG data suggested a phase change to a centrosymmetric structure at $T_C \approx 590$ °C. Therefore, Rietveld refinement of the elevated temperature powder neutron diffraction data was carried out with refinements in space group *P*2*an* for $T = 550$ °C and below, and *P*4/*mmm* for $T > 550$ °C. The relationship of the anticipated 'parent' paraelectric tetragonal phase to the ferroelectric orthorhombic phase is $a_O \sim b_O \sim \sqrt{2}a_T$, directly analogous to that in the Aurivillius phases.

The variation of lattice parameters derived from these refinements is shown in Fig. 6 and 7. A gradual merging of *a* and *b* parameters, followed by a sharp coalescence near T_C, is observed, together with a discontinuous change in the *c* parameter at the same temperature. This suggests a somewhat smeared first-order ferroelectric–paraelectric phase transition, which is supported by the plot of an order parameter, $Q (= \varepsilon^{1/2})$, based on orthorhombic strain, $\varepsilon = [2(a - b)/(a + b)]$, *versus*

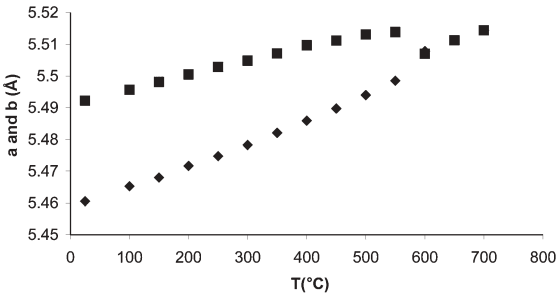

Fig. 6 Variation of *a* (■) and *b* (◆) lattice parameters *versus* temperature.

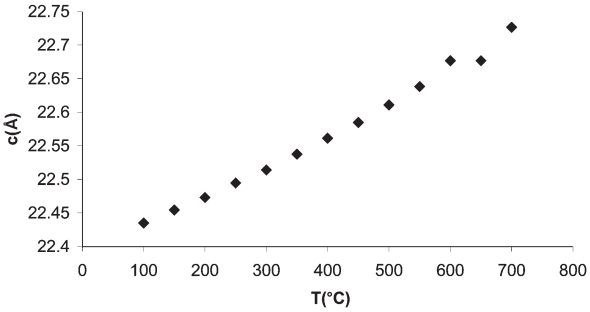

Fig. 7 Variation of *c* lattice parameter *versus* temperature.

Table 4 Final atomic parameters for $Bi_5PbTi_3O_{14}Cl$ at 600 °C; space group *P4/mmm*, $a = 3.89371(7)$, $c = 22.6747(5)$ Å, $\chi^2 = 1.00$, $R_{wp} = 0.011$ for 44 variables

Atom	*x*	*y*	*z*	$U(11)/Å^2$	$U(22)/Å^2$	$U(33)/Å^2$
Bi(1)	0.0	0.0	0.4126(1)	0.015(1)	0.015(1)	0.027(2)
Bi(2)	0.5	0.5	0.0969(2)	0.051(1)	0.051(1)	0.061(2)
Bi(3)	0.5	0.5	0.3008(2)	0.038(1)	0.038(1)	0.033(2)
Ti(1)	0.0	0.0	0.0	0.020(3)	0.020(3)	0.000(3)
Ti(2)	0.0	0.0	0.1851(2)	0.005(1)	0.005(1)	0.032(3)
Cl(1)	0.5	0.5	0.5	0.044(2)	0.044(2)	0.059(3)
O(1)	0.0	0.0	0.0851(2)	0.073(2)	0.073(2)	0.015(2)
O(2)	0.0	0.0	0.2636(2)	0.075(2)	0.075(2)	0.020(3)
O(3)	0.5	0.0	0.0	0.010(2)	0.075(4)	0.069(4)
O(4)[a]	0.5	0.0	0.1700(2)	0.014(1)	0.038(2)	0.052(2)
O(5)[b]	0.5	0.0	0.3620(1)	0.011(1)	0.029(1)	0.022(1)

[a]Equivalent to O(5) and O(6) in *P2an*. [b]Equivalent to O(4) and O(7) in *P2an*.

temperature shown in Fig. 8. Using a simple Landau model,[25] the three parameters $Q(0) = 0.0768$, $T_C = 591$ °C and critical exponent, $\beta = 0.14$, can be derived, where

$$Q(T) = Q(0)[(T_C - T)/T]^{\beta}$$

This behaviour is very similar to that in $Bi_4Ti_3O_{12}$ itself,[18] but contrasts significantly with both the 'even-layer' Aurivillius phases $Sr_{0.85}Bi_{2.1}Ta_2O_9$[21] and $SrBi_4Ti_4O_{15}$,[22] and the A1X1 phase Bi_4TaO_8Cl.[11] In these cases, an intermediate paraelectric orthorhombic phase is present between the ferroelectric orthorhombic and paraelectric tetragonal phases. There is no evidence from our powder neutron diffraction data for such a phase in the present case. In particular, a careful examination of the 550 °C data suggests no elevation of symmetry to *C2mm*, for example, and the 600 °C data suggests no deviation from tetragonality. The final Rietveld fit for the 600 °C refinement in *P4/mmm* is shown in Fig. 9.

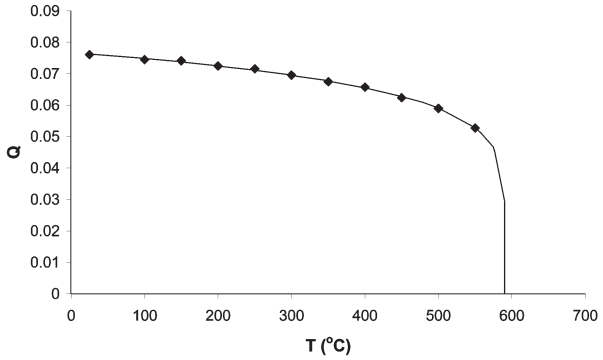

Fig. 8 Plot of order parameter, *Q*, *vs.* temperature. The solid line (intended as a guide to the eye only) represents the least-squares fit to a Landau model with critical exponent $\beta = 0.14$.

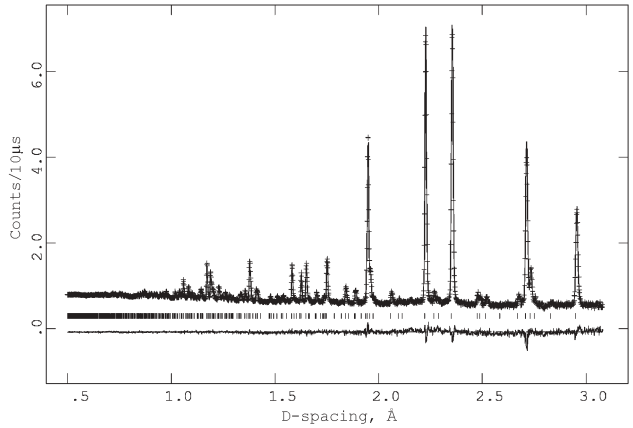

Fig. 9 Final Rietveld plot for $Bi_5PbTi_3O_{14}Cl$ at 600 °C; space group *P4/mmm*.

Final refined atomic parameters and bond distances for the *P4/mmm* phase at 600 °C are given in Tables 4 and 5. A comparison of this paraeletric phase with the corresponding high temperature phase for $Bi_4Ti_3O_{12}$[17] shows some interesting similarities and differences. The two Ti environments in both cases are very similar, both 'outer' Ti(2) sites showing the same off-centre displacement towards the apical oxygen adjacent to the $[Bi_2O_2]$ layers. The degree of this distortion is very similar in both paraelectric phases (for $Bi_4Ti_3O_{12}$, the corresponding Ti–O bond lengths are 1.74 and 2.34 Å) and does not differ greatly from those of the room temperature phase given in Table 2. The environment of the A site of the perovskite block is also very similar in the two paraelectric phases [the values for $Bi_4Ti_3O_{12}$ corresponding to the Bi(2)–O distances shown in Table 5 are 2.75, 2.96 and 2.55 Å, respectively]. In both cases, the Bi shows a significant shift away from the central Ti(1)–O(3) layer and towards the outer Ti(2)–O(4) layer. The Bi environments for the $[Bi_2O_2]$ layer sites, on the other hand, show some differences, which may be due to the accommodation of the additional [Cl] layer. In $Bi_4Ti_3O_{12}$, the Bi–O(layer) distance is 2.32 Å and the Bi–O(apical) distance is 2.91 Å. In $Bi_5PbTi_3O_{14}Cl$, the Bi–O(layer) distances are correspondingly longer for Bi(3) and shorter for Bi(1), the latter in order to accommodate the relatively weak bonding to the halide layer.

Conclusions

We have established that the regular A3X1 phase $Bi_5PbTi_3O_{14}Cl$ can be prepared in bulk polycrystalline form. The basic structural features of this phase are those expected for the suggested Sillén–Aurivillius intergrowth, with layer sequence $\cdots[M_2O_2][M_2Ti_3O_{10}][M_2O_2][Cl]\cdots$. In detail, this structure is polar at room temperature, though there are significant differences between the perovskite blocks within this phase and that of the 'parent' A3 phase $Bi_4Ti_3O_{12}$, caused by accommodation of the Sillén block. These differences lead to a somewhat lower T_C and smaller SHG and permittivity values compared to $Bi_4Ti_3O_{12}$. A single structural phase transition *P2an* → *P4/mmm* occurs at around 590 °C, coincident with T_C. This parallels the behaviour of $Bi_4Ti_3O_{12}$ and contrasts with that of the A2 and A4 phases $SrBi_2Ta_2O_9$ and $SrBi_4Ti_4O_{15}$,

Table 5 Selected bond distances (Å) for $Bi_5PbTi_3O_{14}Cl$ at 600 °C

Ti(1)–O(1) × 2	1.930(4)	Bi(2)–O(1) × 4	2.766(1)
Ti(1)–O(3) × 4	1.947(1)	Bi(2)–O(3) × 4	2.936(1)
Ti(2)–O(1)	2.266(7)	Bi(2)–O(4) × 4	2.556(4)
Ti(2)–O(2)	1.780(7)		
Ti(2)–O(4) × 4	1.977(1)	Bi(3)–O(2) × 4	2.880(2)
		Bi(3)–O(5) × 4	2.392(2)
Bi(1)–Cl(1) × 4	3.392(2)		
Bi(1)–O(5) × 4	2.259(2)		

respectively, both of which show an intermediate paraelectric phase. The three Sillén–Aurivillius intergrowth phases that we have studied in detail so far, *viz.* Bi_4TaO_8Cl (A1X1), $Bi_3Pb_2Nb_2O_{11}Cl$ (A2X1) and the present material, show considerable differences in both their structural and electrophysical behaviour, thus prompting further studies of related materials in order to further understand the structure–composition–property relationships within this complex family, and their relationship to the Aurivillius phases.

Acknowledgements

We would like to thank INTAS and the Royal Society/NATO for awards to A. M. K. and the EPSRC for provision of neutron facilities at ISIS. We thank Dr R. I. Smith and Dr C. Hervoches for help with the neutron data collection. and Mrs S. Williamson for the DTA measurements.

References

1 B. Aurivillius, *Ark. Kemi*, 1949, **1**, 499.
2 C. A. P. de Araujo, J. D. Cuchiaro, L. D. McMillan, M. C. Scott and J. F. Scott, *Nature (London)*, 1995, **364**, 627.
3 B. A. Popovkin, A. M. Kusainova, V. A. Dolgikh and L. G. Aksel'rud, *Russ. J. Inorg. Chem.*, 1998, **43**, 1471.
4 V. A. Dolgikh and L. N. Kholodkovskaya, *Russ. J. Inorg. Chem.*, 1992, **37**, 488.
5 K. D. M. Harris, W. Ueda and J. M. Thomas, *Angew. Chem., Int. Ed. Engl.*, 1988, **27**, 1364.
6 D. O. Charkin, P. S. Berdonosov, A. M. Moisejev, R. R. Shagiakhmetov, V. A. Dolgikh and P. Lightfoot, *J. Solid State Chem.*, 1999, **147**, 527.
7 J. F. Ackerman, *J. Solid State Chem.*, 1986, **62**, 92.
8 B. Aurivillius, *Chem. Scr.*, 1984, **23**, 143.
9 A. M. Kusainova, S. Yu. Stefanovich, V. A. Dolgikh, A. V. Mosunov, C. H. Hervoches and P. Lightfoot, *J. Mater. Chem.*, 2001, **11**, 1141.
10 A. M. Kusainova, P. Lightfoot, W. Zhou, S. Yu. Stefanovich, A. V. Mosunov and V. A. Dolgikh, *Chem. Mater.*, 2001, **13**, 4731.
11 A. M. Kusainova, W. Zhou, J. T. S. Irvine and P. Lightfoot, *J. Solid State Chem.*, 2002, **166**, 148.
12 A. S. Bhalla, R. Guo and R. Roy, *Mater. Res. Innovations*, 2000, **4**, 3.
13 D. Y. Suarez, I. M. Reaney and W. E. Lee, *J. Mater. Res.*, 2001, **16**, 3139.
14 A. C. Larson and R. B. von Dreele, Los Alamos National Laboratory Report No. LA-UR-86-748, Los Alamos, NM, USA, 1987.
15 V. I. Voronkova and V. K. Yanovskii, *Phys. Status Solidi*, 1987, **101**, 51.
16 A. D. Rae, J. G. Thompson, R. L. Withers and A. C. Willis, *Acta Crystallogr., Sect. B*, 1990, **46**, 474.
17 C. H. Hervoches and P. Lightfoot, *Chem. Mater.*, 1999, **11**, 3359.
18 P. Lightfoot and C. H. Hervoches, *Proceedings of CIMTEC, 10th International Ceramics Congress, Florence, July 2002*, Techna, Faenza, in press.
19 A. M. Glazer, *Acta Crystallogr., Sect. B*, 1972, **28**, 3384.
20 A. D. Rae, J. G. Thompson and R. L. Withers, *Acta Crystallogr., Sect. B*, 1992, **48**, 418.
21 C. H. Hervoches, J. T. S. Irvine and P. Lightfoot, *Phys. Rev. B.*, 2001, **64**, 100102(R).
22 C. H. Hervoches, A. Snedden, R. Riggs, S. H. Kilcoyne, P. Manuel and P. Lightfoot, *J. Solid State Chem.*, 2002, **164**, 280.
23 R. L. Withers, J. G. Thompson and A. D. Rae, *J. Solid State Chem.*, 1991, **94**, 404.
24 S. C. Abrahams, S. K. Kurtz and P. B. Jamieson, *Phys. Rev.*, 1968, **172**, 551.
25 A. Putnis, *Introduction to Mineral Sciences*, Cambridge University Press, Cambridge, 1992.
26 M. Gillberg, *Ark. Mineral. Geol.*, 1960, **2**, 565.
27 V. Srikanth, H. Idink, W. B. White, E. C. Subbarao, H. Rajagopal and A. Sequeira, *Acta Crystallogr., Sect. B*, 1996, **52**, 432.